Direct experimental identification of the structure of ultrathin films of bcc iron and metastable bcc and fcc cobalt

Hong Li and B. P. Tonner*
Department of Physics, University of Wisconsin–Milwaukee, 1900 East Kenwood Boulevard, Milwaukee, Wisconsin 53211
(Received 6 March 1989)

X-ray-excited photoemission and Auger-electron angular distributions from epitaxial transition-metal films are shown to be characteristic of crystal structure but insensitive to elemental species. This feature is used to identify the structures of ultrathin films of iron and cobalt, grown at room temperature on single-crystal metal substrates. It is found that cobalt grows in the metastable bcc Co(001) structure on bcc Fe(001) thin films, and fcc Co(001) grows on fcc Cu(001). While bcc Fe(001) can be stabilized on fcc Ag(001) substrates, this is not the case for cobalt films. Epitaxy of cobalt on Ag(001) results in a complex structure that is neither fcc nor bcc but is consistent with a body-centered tetragonal structure. These results are used to determine an upper bound on the strain that bcc cobalt films can sustain in room-temperature growth.

I. INTRODUCTION

Epitaxial growth under ultrahigh-vacuum conditions is an important technique for the creation of new phases of materials.[1] In the case of transition-metal film growth, a variety of factors such as interfacial strain and surface free energies are important in determining the structures of the films. An interesting special case of epitaxially stabilized structures is the metastable crystal structures.[2] These are materials with lattice parameters which result in a local minimum in the total free energy, separated from the absolute energy minimum by an activation energy. For such metastable films, the criterion of lattice misfit at the substrate-overlayer interface tends to be more critical than the interface energy in determining whether or not the metastable structure can be grown on a given substrate.[3] For example, while epitaxy of cobalt[4,5] or nickel[6,7] on Cu(100) results in an increase in the surface free energy, both of these elements form well-defined fcc ultrathin films, with lattice-matched pseudomorphic structures.

Cobalt and iron can both be grown in more than one epitaxially stabilized crystal structure. For example, bcc Fe(001) has been previously reported in epitaxy on Ag(100).[8,9] This result is confirmed in this study, which also reports direct structural identification of this phase using the x-ray-excited electron-emission patterns now known as "forward-scattering enhancements."[10] We further find that two metastable phases of cobalt can be epitaxially grown: fcc Co(001) on Cu(001) substrates, and bcc Co(001) on bcc Fe(001) thin films. This is the first demonstration of bcc cobalt growth on a metal substrate.

A prevalent feature of lattice-matched epitaxial growth of these metastable structures on metal substrates is that both the growing film and the underlying substrate share an identical two-dimensional unit cell (1×1 periodicity). This is true both for the case of a fcc overlayer growing on a fcc substrate, as in the case of Co/Cu(001), and for bcc growth on a fcc substrate as in Fe/Ag(001). The difference between these examples lies in the relative orientation of the film and substrate crystallographic axes which are parallel to the interface. In the fcc/fcc case the growth is [110]||[110]; in the bcc/fcc case it is [110]||[100].

The identical unit surface mesh of overlayer and substrate can make an identification of the overlayer structure difficult, since there are no superlattice beams in the electron diffraction pattern which can be unambiguously identified as being due to the overlayer alone.[11] If the film is "ultrathin," then a surface-sensitive structural probe is necessary, preferably one which is available during *in situ* growth and is easy to interpret. Here we define "ultrathin" as implying a film thickness which is near the limit for which three-dimensional band-structure effects arise in photoemission spectroscopy (a few bulk lattice constants perpendicular to the surface). Low-energy electron diffraction (LEED) is routinely used to monitor long-range order in epitaxial growth. However, since LEED is not intrinsically elementally selective, the diffraction pattern and I-V curves reflect the composite structure of both the overlayers and the substrate for the case of (1×1) epitaxial growth. Even a detailed I-V analysis is hampered by the similarity in electron scattering of overlayer and substrate in cases like iron or cobalt on copper substrates.[4,7,12]

In this study, we have employed the recently developed techniques of angle-resolved x-ray photoelectron scattering and Auger-electron scattering (ARXPS and ARAES) to determine the structures of ultrathin films of iron and cobalt.[6,13–15] In addition to possessing the required surface sensitivity, these techniques have the intrinsic capability of distinguishing the structure of the epitaxial film from that of the substrate. In its simplest form, the ARXPS or ARAES angular distributions of electron-emission intensity will have intensity maxima corresponding to the nearest-neighbor bond directions in the sample, which can be used to determine the crystal structure of an ultrathin film.[10,16] Since the technique is

atomic-species specific, it is easy to identify the structure of an ultrathin film on a substrate with the same geometrical structure and similar atomic number. The technique does not require the sample to have long-range order, which makes it complementary to LEED and is useful for probing epitaxial structures during the early stages of growth.

The use of ARXPS in studies of metastable film growth is illustrated in this study of epitaxial cobalt and iron. The similarity in the measured ARXPS angular distributions from fcc Co(100), Cu(100), and Ag(100) is used to argue that these angular distributions are *chemically independent* under certain conditions. The angular distributions from fcc Cu(001) and bcc Fe(001) are used to "fingerprint" the structures of epitaxial cobalt films. The observation that cobalt forms in the bcc structure on iron substrates but not on Ag(100) (even though bcc Fe *does* grow on this substrate) is used to place an upper bound on the strain which can be sustained by metastable bcc cobalt ultrathin films.

II. EXPERIMENTAL APPROACH

Single-crystal Cu(100) and Ag(100) substrates were oriented by Laue diffraction to within $\frac{1}{2}°$ for spark planing, followed by mechanical polishing. These substrates were subsequently cleaned by repeated cycles of argon ion bombardment followed by high-temperature annealing. Sample cleanliness was determined by Auger-electron spectroscopy (AES) and x-ray photoelectron spectroscopy (XPS). The principle surface contaminants for both the Cu and Ag substrates were C and O, and were reduced to less than 2% (1%) of a monolayer (ML) for Ag (Cu), as monitored by XPS and electron-excited AES. Surface ordering was monitored by LEED. The experiments were performed in a multichamber ultrahigh-vacuum system which permits *in situ* film deposition and characterization.[17,18] This system contains two main functional units, a growth chamber and an analysis chamber, connected by an ultrahigh-vacuum transfer line which moves the sample from the growth region to the analysis region. The growth chamber is based upon a 300-mm-diam sphere (14-1 volume), and is equipped with a 220-l/s ion pump, 150-l/s turbomolecular pump, and cryotrapped Ti-sublimation pump, in addition to the liquid-nitrogen cryoshields surrounding a set of three evaporation sources. Before filling the liquid-nitrogen traps, the base pressure of the growth chamber is typically less than 2.0×10^{-10} Torr (as monitored over a one-month period). The analysis chamber, which contains the apparatus for ARXPS,[17] has a base pressure of $8-9\times10^{-11}$-Torr range before filling an additional cryotrap located in this chamber. Residual gases, and purity of the argon sputtering gas, are monitored using a quadrupole mass spectrometer.

All-metal evaporation sources were used for depositing pure overlayer films. The cobalt source was a resistively heated wire of 99.99% purity. The iron source was a 99.997% purity iron wrapped around a resistively heated tungsten wire. During depositions the substrates were at room temperature. The deposition rate was controlled by measuring the source temperatures using either thermocouples (Fe/W source) or an optical pyrometer (Co). The evaporation rates were determined by deposition onto a quartz crystal microbalance mounted on a removable sample holder which could be placed at the same position as the substrates. Plots of film thickness as measured by the quartz microbalance were made as a function of time for periods from 10–30 min to verify the long-term stability of the deposition rate. The coverages reported here were calculated from the microbalance deposition rate measurement, scaled for the appropriate deposition time. Deposition rates were chosen to be approximately 0.75–1.0 ML per minute. The evaporation sources were outgassed until pressures during deposition remained below 4×10^{-10} Torr.

The angle-resolved XPS and AES measurements were performed in a geometry in which the angle between the incident unpolarized x-ray beam and the outgoing electron was fixed at $\approx75°$. Both Al and Mg $K\alpha$ radiation were used. Azimuthal orientation of the crystal surface was done by reference to the LEED pattern. Polar-angle-dependent photoelectron or Auger-electron intensities were measured at fixed azimuthal angles chosen to place the emitted electron in a high-symmetry plane of the overlayer. Angular scans were performed by rotating the sample in steps of 0.2°, and accumulating electron intensities simultaneously in two bands of kinetic energies corresponding to XPS (or AES) peaks and background regions. The angular resolution of the electron detector was $\pm2.5°$ in polar angle and $\pm3°$ in azimuthal angle. Reproducibility of the measured angles corresponding to intensity maxima in the angle-dependent electron intensity distributions has been checked by comparing single-crystal Cu(100) curves taken at various times during the experimental run, and was found to be $<1.0°$.[16]

III. CHEMICAL INDEPENDENCE OF PHOTOEMISSION FORWARD SCATTERING

It has been known since the work of Fadley and Bergström on single-crystal gold substrates that the emission intensity of high-energy photoelectrons is highly anisotropic, due to the underlying crystal structure.[13] Recent measurements confirm a theoretical model that shows that the major intensity maxima correspond to strings of atoms in the solid lying along high-symmetry directions.[16] This "forward-focusing" model predicts that the highest emission yield is actually along the directions with highest atom density, a phenomenon which can be explained by multiple-scattering effects.[6,10] The forward-focusing peaks of ARXPS are also seen in the corresponding x-ray-excited *Auger*-electron scattering (ARAES),[15] since the dominant contribution to the effect is the electron scattering of the outgoing electron.

We have found that ARXPS (or ARAES) is a useful technique for rapidly and unambiguously determining the crystal structure of simple-cubic ultrathin films as a function of film thickness. The particular utility of the technique is that a qualitative interpretation of the data is relatively straightforward, although a quantitative reproduction of the angular distribution might require a full

multiple-scattering calculation. In our study of transition-metal film growth, we find that the ARXPS angular distributions are similar for different materials with the same structure, a feature we call chemical independence. Different structures of the same material, however, produce radically different ARXPS patterns.

This principle is illustrated by our study of the growth of fcc cobalt films on Cu(100). Cobalt grows epitaxially in a nearly ideal layer-by-layer mode as a fcc structure oriented with axes parallel to the Cu(100) substrate.[18] The evolution of the forward-scattering angular distributions for the cobalt overlayer and copper substrate $2p_{3/2}$ core levels is shown in Fig. 1, as a function of the overlayer thickness in units of cobalt monolayers. Note the similarity of the thick cobalt film angular distribution (top right) to the initial copper substrate curve (lower left). Along the [100] azimuth shown, there are two major forward-scattering enhancements present: a normal emission peak (0°) and a peak at 45° polar angle. The thick cobalt film quantitatively reproduces these features to within experimental uncertainty. Similar results are found for measurements along the [110] azimuth.

We have used ARXPS, as well as conventional measurements of photoemission intensity as a function of coverage, to determine in detail the growth mode of cobalt on Cu(100).[18] We find only minor deviations from ideal layer-by-layer growth at low coverages. Specifically, from ARXPS angular distributions along the [100] and [110] azimuths, we find evidence for the formation of two-layer-thick islands up to the point at which deposition of two equivalent monolayers causes the islands to coalesce. This initial stage is followed with layer-by-layer epitaxy. A sharp 1×1 LEED pattern persists up to approximately 10 ML thickness, indicating that long-range order in these films is still present. Due to the similar electron scattering properties of cobalt and copper, there are no significant differences expected in the LEED energy dependence from fcc Co(100) and fcc Cu(100).[4] Therefore a direct identification of the crystal structure of the overlayer is difficult using LEED alone.

The chemical specificity of the photoelectron forward-scattering angular distribution, however, makes this identification unambiguous. As noted also in the case of iron epitaxy (below), the forward-scattering enhancements sense a short-range order than that of the LEED pattern, so that the two measurements combined are complementary. In the case of metastable fcc Co/Cu(100), the sharp LEED pattern with low background implies good long-range order, and the photoelectron forward scattering identifies the structure as fcc with overlayer and substrate axes being parallel.

As an example of a rather extreme test of the chemical independence of forward-scattering angular distributions, we show in Fig. 2 the ARXPS pattern along a principle azimuth from Ag(100) in comparison to the ARAES distribution for Cu(001). The fcc structure shared by these

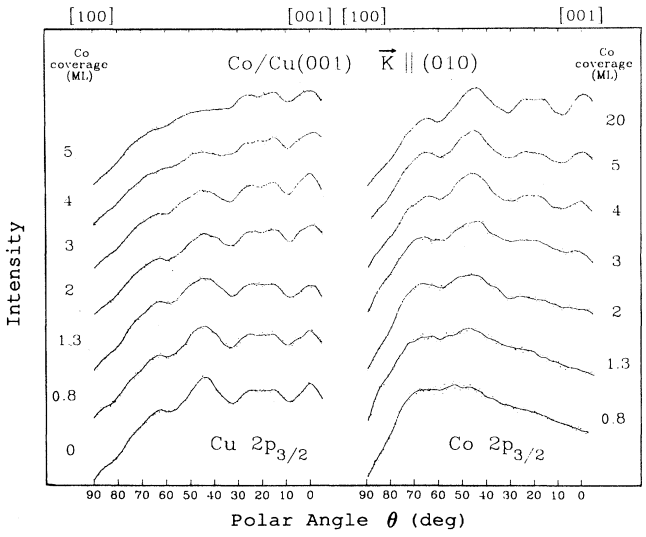

FIG. 1. Photoelectron intensity angular distributions from the Cu substrate and Co thin film as a function of overlayer coverage. The plotted intensity has a background due to inelastic electron scattering subtracted. The fall off in intensity at large polar angles (grazing electron exit angle) is due to geometric factors. Distributions for different coverages are scaled to have the same amplitude at normal emission for purposes of comparison.

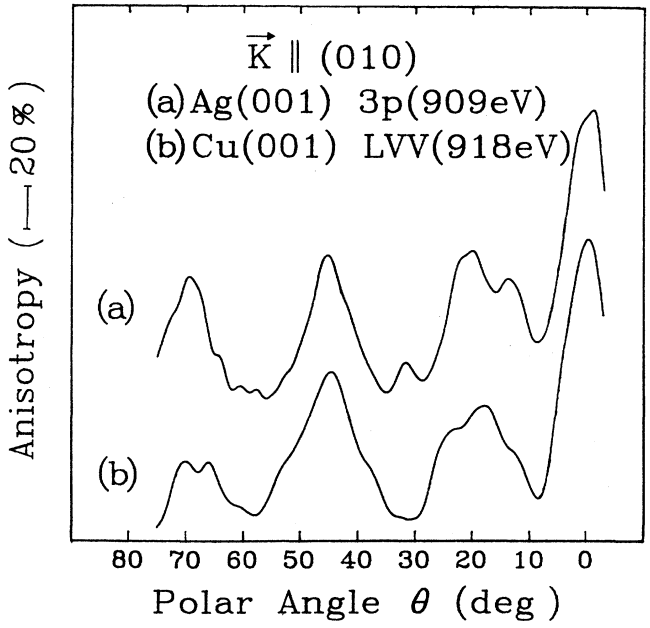

FIG. 2. Emitted electron angular distributions from bulk silver and copper, along identical azimuths. The electron kinetic energy in each case is shown in parentheses. The intensities are plotted as angular anisotropy, derived by dividing the actual intensity by the background due to inelastically scattered electrons, so as to suppress smoothly varying geometric features. In the absence of forward-scattering enhancements, the anisotropy would be independent of polar angle.

substrates produces the large peaks at normal emission and at 45° polar angle, corresponding to the [001] and [101] crystal directions. Broader characteristic peaks near [103] (18.4°) and [301] (71.6°) are also present in both samples, although these peaks are affected by multiple-scattering "side lobes" associated with the primary scattering along [001] and [101].[10] Despite the large difference in atomic number, lattice constant, and the source of electrons (photoemission versus Auger emission), these curves show a strong resemblance which easily identifies them as belonging to a fcc crystal. The major constraint which must be satisfied to allow comparison between the angular distributions from different elements is to use electrons with similar kinetic energy, preferably of order 1 keV or higher.[10] This can be accomplished, for example, by varying the incident photon energy to compensate for differences in electron binding energy.

The concept of chemical independence of ARXPS angular distributions has been implicitly used in other studies of transition-metal film growth. Examples can be found in a study of Co/Ni(001) epitaxy by Chambers *et al.*[15] and in a study of the Cu-Ni system by Armstrong and Egelhoff.[19]

IV. METASTABLE STRUCTURE OF EPITAXIAL bcc AND fcc Co

We have used the forward-scattering model of ARXPS and ARAES to determine the structure of Fe and metastable Co epitaxial films. We studied the epitaxially stabilized bcc phases of Fe and Co, and the fcc metastable form of Co. The room-temperature equilibrium phase of Fe is bcc, so epitaxy in this case results in a simple strained-layer film. The equilibrium structure of cobalt at room temperature is hcp, so that room-temperature epitaxially stabilized fcc and bcc films are "true" metastable structures.

It has been proposed, through indirect arguments based upon lattice matching, that the structure of iron films on fcc Ag(001) substrates is the bcc phase.[8] The lattice-matching argument is based on the fact that the size of the two-dimensional surface mesh of Ag(001) is close to that of bulk bcc Fe(001), if the two crystals are rotated so that the fcc [001] direction is parallel to the bcc [011] direction in the interface plane.

A model of this composite structure is shown in Fig. 3. Note that the only difference between the fcc substrate and bcc overlayers is the interlayer spacing, which is smaller in the bcc structure. For a bulk crystal, this contraction along [001] could result from a uniaxial compression along the sample normal. However, in the present case, it is the result of the Ag(100) lattice requiring a *larger* lattice spacing in the plane than can be accommodated by fcc iron. The fcc→bcc transformation can be explained simply by a hard-sphere model, in which the bcc phase is the direct result of expansion of the lattice parameter parallel to the interface, while the atomic radius remains constant.

The substrate-film interface is still of 1×1 periodicity, so that this structure cannot be explicitly determined by simple observation of the LEED pattern. The ambiguity inherent in interpreting the LEED pattern from Fe/Ag(100) previously led to an incorrect identification of this system as being a highly strained *fcc* iron overlayer.[11] Therefore the first objective of this study was to measure the ARXPS patterns from epitaxial Fe/Ag(001) to provide direct experimental evidence for the structure of the bcc phase. As shown below, our results confirm that Fe is in the bcc phase on Ag(100), as conjectured originally by Jonker and Prinz on the basis of lattice-matching arguments.[20]

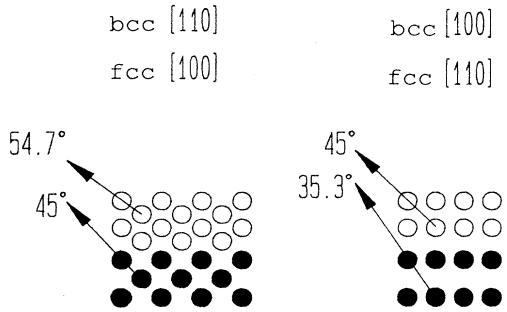

FIG. 3. Model of bcc-fcc epitaxial growth structure appropriate for the Fe/Ag and Co/Ag systems. The principle forward-scattering enhancement directions are shown for two high-symmetry azimuths. The bcc overlayer can be viewed as resulting from a biaxial expansion of a fcc structure parallel to the interface with the substrate.

Given that bcc iron forms on Ag(001), we attempted to grow bcc cobalt on the same surface. However, the cobalt films on silver substrates produced ARXPS patterns which were different from both those of fcc and bcc structures. In striking contrast, growth of cobalt on a bcc iron *film* does produce a bcc structure. Previous work has shown that bcc cobalt and iron can be grown on semiconductor surfaces of GaAs(110).[21] Therefore the current work is important in demonstrating the capability to produce room-temperature bcc cobalt on metal substrates, for which the growth mode results in the formation of well-defined few-layer films.

In addition, the fcc metastable phase of cobalt has been grown on Cu(001) and identified using the ARXPS technique. Growth of fcc cobalt on fcc Cu(001) occurs with all overlayer and substrate lattice directions being parallel, in contrast to the bcc/fcc case discussed above. An in-depth report of the growth mode of cobalt on this substrate will appear elsewhere.[22]

A combination of LEED and photoemission forward-scattering angular distributions was used to determine the structure of Fe ultrathin films on Ag(100). The results for the forward-scattering enhancements from the Fe $2p_{3/2}$ core level are shown in Figs. 4 and 5. It is immediately apparent from these curves that iron grows in the bcc structure, with (bcc [110])||(fcc [100]). To see this, consider the forward-scattering peaks in the Ag(001) [100] azimuth (Fig. 4). According to the accompanying structure model, a fcc film would show forward-

scattering enhancements at angles of 0°, 18.4°, and 45°, as is seen in the previous examples for fcc Cu, Co, and Ag (Figs. 1 and 2). Instead, the major enhancement features occur at 0°, 25°, and 55°, as appropriate for a bcc structure.

Similarly, along the Ag(100) substrate [110] azimuth (Fig. 5), strong enhancement features at normal emission, 25°, 45°, and ≈66° correspond to the bcc directions shown in the model. A comparison of the intensity dependence of the Fe enhancement peaks as film thickness increases can be used to infer the growth mode. In particular, for a 2-ML-equivalent deposition, there is a peak in the Ag [100] azimuth at 55° (bottom curve in Fig. 4) which is due to scattering between two successive layers of iron. However, no enhancement is seen at 45° along Ag [110], which means that there are no three-layer-thick islands formed when 2-ML equivalent of iron is deposited. This is a strong indication of layer-by-layer growth mode.

The LEED pattern was monitored at stages during iron epitaxy. Typical diffraction patterns are shown in Fig. 6. For films of 2- and 3.5-ML-equivalent thickness the LEED pattern remained visible with a 1×1 pattern and increasing background intensity. At 5 ML thickness, the spots are obscured by a substantial background, indi-

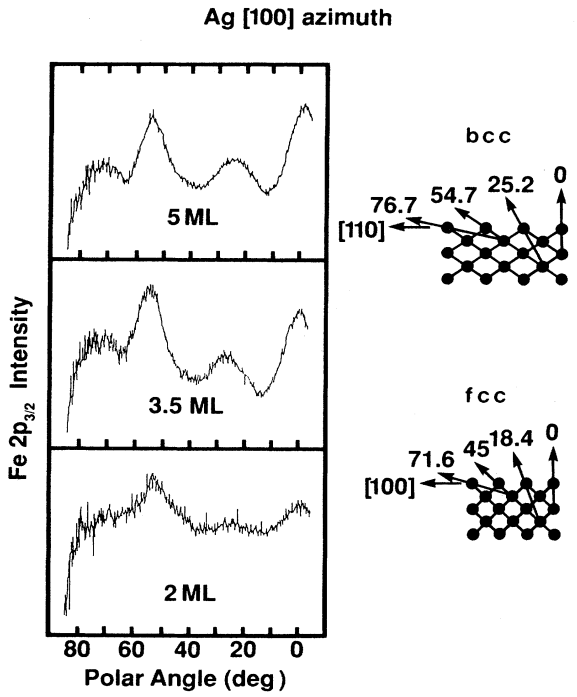

FIG. 4. Photoemission angular distributions from bcc Fe(100) thin films grown on Ag(100), along the substrate [100] azimuth. The bcc structure can be readily identified by the prominent forward-scattering feature at 55°. As shown in the accompanying models, this peak would be shifted to 45° in a fcc lattice. The angular distributions shown are anisotropies, as for Fig. 2.

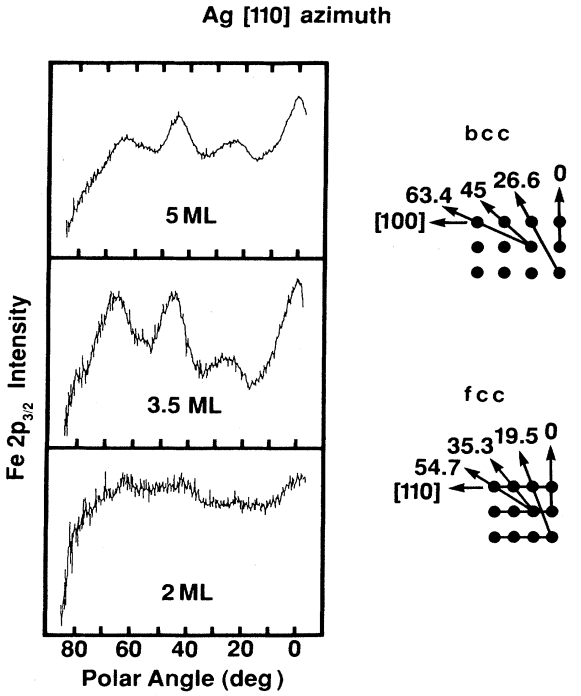

FIG. 5. As for Fig. 4, but along the substrate [110] azimuth. The large forward-scattering peak at 45° requires 3-ML film thicknesses or larger. The absence of this feature at 2-ML coverage implies a layer-by-layer growth mode.

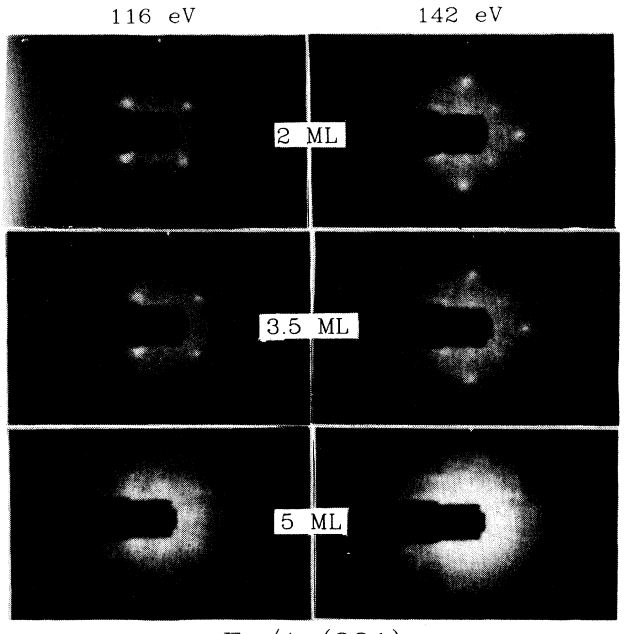

FIG. 6. Low-energy electron diffraction patterns from ultrathin iron films on Ag(001) for some selected overlayer thicknesses.

cating a loss of long-range order. In contrast, however, the forward-scattering enhancements are still quite strong at these coverages. This means that the local bcc ordering is preserved. The conventional LEED apparatus used is not sensitive to long-range order beyond a few hundred angstroms, so the absence of LEED spots indicates domain sizes much smaller than this limit. The effective coherence length of the forward-scattering enhancement has not been directly determined for disordered systems, but it can be inferred to be only a few lattice constants long from single-crystal computations and experiments.[10,16] This suggests that the iron films at higher coverages consist of small clusters of bcc Fe with little long-range ordering of the clusters.

The epitaxy of cobalt is different from that of iron in several respects. A comparison of the angular distributions from several cobalt and iron ultrathin films is shown in Fig. 7. The angular distribution from Fe grown on Ag(100) has been identified above as being characteristic of the bcc phase, and is now used to fingerprint the bcc structure in cobalt epitaxy. For example, we find that thin (3 ML) films of cobalt grown on the bcc Fe/Ag(100) system exhibit a bcc structure. This is easily demonstrated by comparing the top two pairs of angular distributions [(a) and (b) in Fig. 7)] corresponding to bcc Fe and bcc Co structures.

This case represents a metastable bcc multilayer sandwich consisting of an outer 3-ML bcc cobalt film, on top of a 3.5-ML bcc iron film, grown initially on fcc Ag(100). It is one of the powerful features of the chemical selectivity of photoelectron forward-scattering studies, that the individual structures of each of these elements can be independently verified even though the overall structure is quite complex. While a full theoretical calculation of the angular distributions would enable further interpretation of the structure, it is clear from Fig. 7 that an empirical fingerprinting of simple cubic structures can be accomplished by comparing unknown structures to measured standards.

Since bcc Fe is closely lattice matched to the Ag(100) surface (after a rotation of unit cell by 45°), we attempted to grow bcc cobalt directly on this substrate. The results, shown in Fig. 7 along with the curves for metastable fcc and bcc cobalt, indicate that direct growth of bcc cobalt on Ag(100) does not occur. Instead, a structure is formed with forward-scattering peaks which agree with neither the bcc nor the fcc cobalt structure.

If we assume that the cobalt structure on Ag(100) is a

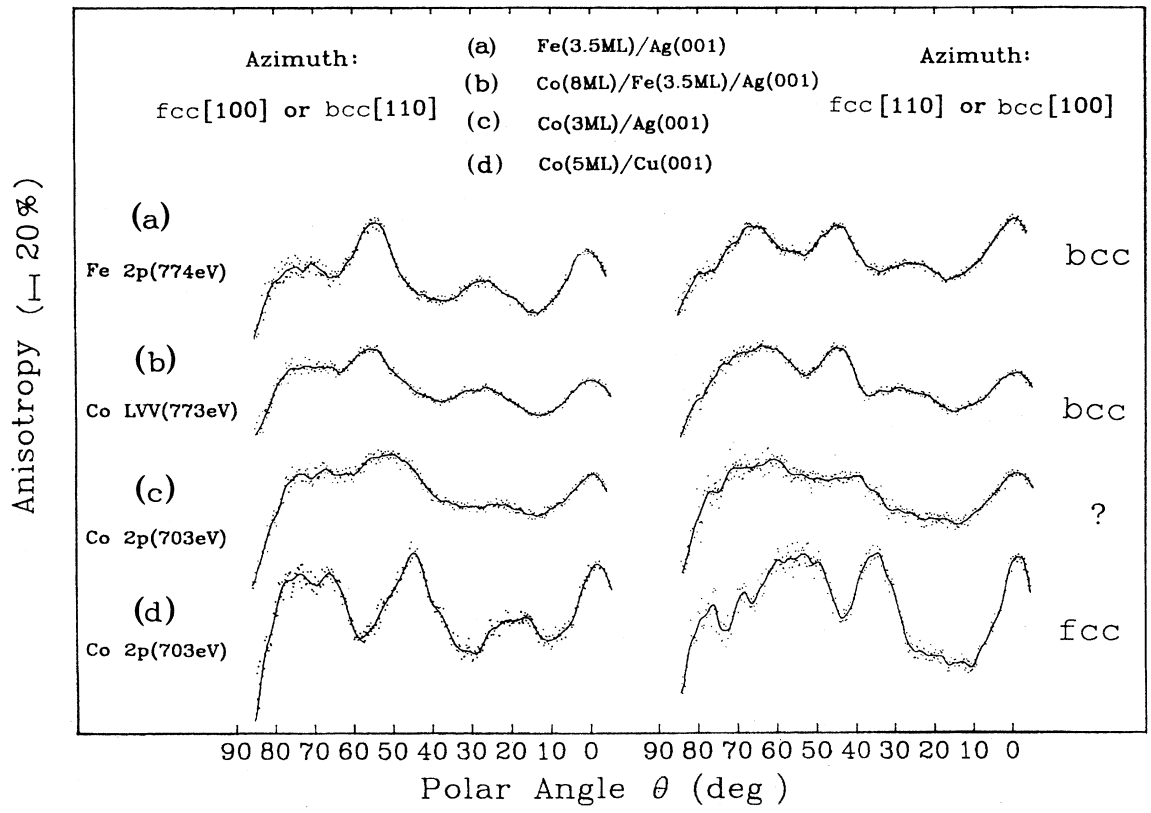

FIG. 7. Photoelectron and Auger-electron angular anisotropy from a series of metastable films.

distortion to the bcc structure, then we can quantify this structure from the (weak) forward-scattering enhancements which are measured. We measure broad features at 50.8° along the Ag[100] azimuth, and 40.9° along Ag[110]. These peaks are in good agreement with a body-centered *tetragonal* (bct) structure, with a lattice-parameter ratio of $|\mathbf{c}|/|\mathbf{a}|=1.15$. To compare this with bcc and fcc structures, let **c** be the thickness of three atomic layers, and **a** be the nearest-neighbor spacing in the surface plane. Then for a fcc film, $|\mathbf{c}|/|\mathbf{a}|=1.41$, and for a bcc film $|\mathbf{c}|/|\mathbf{a}|=1$. The bct Co/Ag(100) film is thus intermediate in structure between fcc and bcc. This highlights the point made earlier, that the bcc structure can be viewed as resulting from a uniaxial compression along the sample normal. The bct structure requires less symmetry than a bcc film, and may therefore be more common than true metastable bcc films.

The epitaxy of cobalt on Ag(100) results in a highly disordered film, since the LEED pattern becomes diffuse, and the amplitude of the forward-scattering enhancements is reduced as compared, for example, to fcc Co/Cu(100). Since the forward-scattering enhancements are already sensitive primarily to short-range order, a weak forward-scattering angular distribution indicates there is little long-range crystalline order in the material.

V. DISCUSSION

We can draw some conclusions regarding the growth mode of metastable cobalt and iron films from the differences in epitaxy between these two materials. The two most significant factors influencing the equilibrium structures in epitaxy are the relative lattice constants of substrate and overlayer and the energy of the interface between them.[3] Although it is difficult to directly measure an interface free energy, some information about this quantity can be inferred from the relative surface tension in the liquid phase of Co and Fe as compared to Ag.[23] The surface tensions of cobalt and iron are very similar, and are about a factor of 2 larger than that of silver. Therefore it is reasonable to propose that the interfacial energies of bcc Fe/Ag and bcc Co/Ag are also very similar. The difference in epitaxy of these two materials, in particular the absence of a metastable bcc Co/Ag(100) phase, cannot be ascribed to differences in interfacial free energy.

This leads us to examine the degree of strain in the bcc thin films, as compared to bulk materials. Epitaxy of bcc iron on Ag(100) results in only a 0.8% strain. The bcc structure of Fe can also be grown on GaAs(110) substrates, with a resultant 1.4% contraction of lattice constant.[24] In contrast, pseudomorphic growth of bcc cobalt on Ag(100) would require a 2.5% strain as compared to bulk. In this case, the lattice constant of "bulk" bcc cobalt (which does not exist in free form) is extrapolated from data on Fe-Co alloys, as suggested by Prinz.[21]

Co(100) films in bcc form can be grown on GaAs(110) and on bulk Fe(100); in both cases the strain is 1.6% or less. The absence of bcc growth of cobalt directly on Ag(100), which requires 2.5% strain in pseudomorphic growth, implies an upper limit in the range of 2% strain, above which the bcc lattice will not grow. Recent measurements by Heinrich *et al.*[25] have found that nickel forms an epitaxial bcc film directly on Ag(100); they have also studied Ni/Fe/Ag(100) multilayers. Their results on the reflection high-energy electron diffraction from such multilayers were interpreted as showing that the bcc Ni films sustain a 2% strain of the in-plane lattice constant, which is in accord with our similar results for Co/Fe/Ag(100) multilayers. Egelhoff and Jacob recently found that forward-scattering enhancements show bcc metastable formation of Cu on Ag(100), but report an "intermediate" structure between fcc and bcc for Mn/Ag(100).[26] Our results for Co/Ag(100) films suggest that Mn and Co may share similar epitaxial bct structures on silver substrates.

Finally, we note that these results apply only to room-temperature depositions. It is likely that the growth modes of these metastable materials depend sensitively on kinetics, so that factors such as differing substrate temperature, growth rate, and substrate surface defect density may substantially alter the limits to metastable bcc film thickness and strain implied by this work.

ACKNOWLEDGMENTS

This work was supported by the National Science Foundation, Division of Materials Research Grant No. DMR-88-05171.

*Corresponding author.

[1]A. S. Arrott, B. Heinrich, S. T. Purcell, J. R. Cochran, and K. B. Urquhart, J. Appl. Phys. **61**, 3721 (1987).

[2]V. L. Moruzzi, Phys. Rev. Lett. **57**, 2211 (1986); V. L. Moruzzi, P. M. Marcus, K. Schwarz, and P. Mohn, Phys. Rev. B **34**, 1784 (1986).

[3]R. Bruinsma and A. Zangwill, J. Phys. (Paris) **47**, 2055 (1986).

[4]A. Clarke, G. Jennings, R. F. Willis, P. J. Rous, and J. B. Pendry, Surf. Sci. **187**, 327 (1987).

[5]A. J. Federenko and R. Vincent, Philos. Mag. **24**, 55 (1971).

[6]W. F. Egelhoff, Jr., Phys. Rev. Lett. **59**, 559 (1987).

[7]M. A. Abu-Joudeh, B. M. Davies, and P. A. Montano, Surf. Sci. **171**, 331 (1986).

[8]N. C. Koon, B. T. Jonker, F. A. Volkening, J. J. Krebs, and G. A. Prinz, Phys. Rev. Lett. **59**, 2463 (1987); B. T. Jonker and G. A. Prinz, Surf. Sci. **172**, L568 (1986).

[9]M. Stampanoni, A. Vaterlaus, M. Aeschlimann, and F. Meier, Phys. Rev. Lett. **59**, 2483 (1987).

[10]H. C. Poon and S. Y. Tong, Phys. Rev. B **30**, 6211 (1984).

[11]G. C. Smith, H. A. Padmore, and C. Norris, Surf. Sci. **119**, L287 (1982).

[12]Z. Q. Wang, S. H. Lu, Y. S. Li, F. Jona, and P. M. Marcus, Phys. Rev. B **35**, 9322 (1987); Z. W. Wang Y. S. Li, F. Jona, and P. M. Marcus, Solid State Commun. **61**, 623 (1987).

[13]C. S. Fadley and S. Å. L. Bergström, Phys. Lett. **35A**, 375 (1971).

[14]J. Osterwalder, E. A. Stewart, D. Cyr, C. S. Fadley, J. Mustre de Leon, and J. J. Rehr, Phys. Rev. B **35**, 9859 (1987).
[15]S. A. Chambers, S. B. Anderson, H.-W. Chen, and J. H. Weaver, Phys. Rev. B **35**, 2592 (1987).
[16]H. Li and B. P. Tonner, Phys. Rev. B **37**, 3959 (1988).
[17]Y. C. Chou, M. J. Robrecht, and B. P. Tonner, Rev. Sci. Instrum. **58**, 1164 (1987).
[18]H. Li, Ph.D. thesis, University of Wisconsin–Milwaukee, 1988 (unpublished).
[19]R. A. Armstrong and W. F. Egelhoff, Jr., Surf. Sci. **154**, L225 (1985).
[20]B. T. Jonker and G. A. Prinz, Surf. Sci. **172**, L568 (1986).
[21]G. A. Prinz, Phys. Rev. Lett. **54**, 1051 (1985).
[22]H. Li and B. P. Tonner (unpublished).
[23]A. Zangwill, *Physics at Surfaces* (Cambridge University Press, Cambridge, 1988), Chap. 1.
[24]G. A. Prinz and J. J. Krebs, Appl. Phys. Lett. **39**, 397 (1981).
[25]B. Heinrich, S. T. Purcell, J. R. Dutcher, K. B. Urquhrat, J. F. Cochran, and A. S. Arrott, Phys. Rev. B **38**, 12 879 (1988).
[26]W. F. Egelhoff, Jr. and I. Jacob, Phys. Rev. Lett. **62**, 921 (1989).

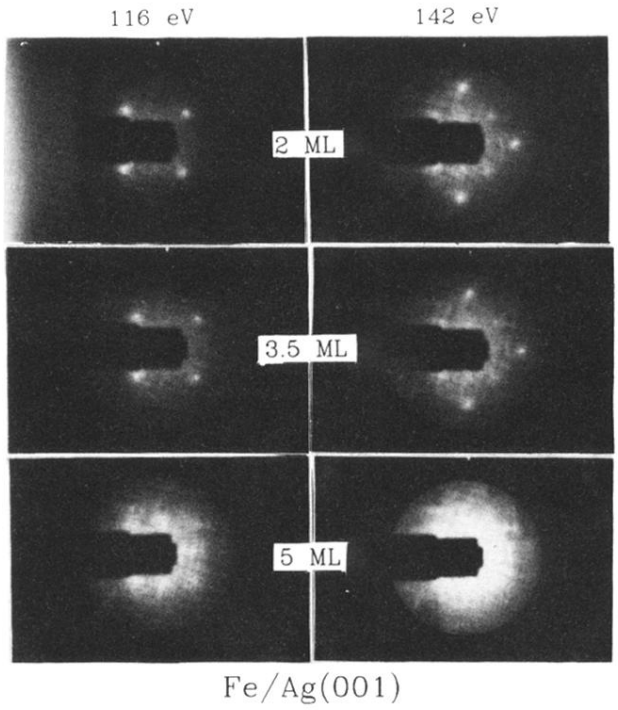

FIG. 6. Low-energy electron diffraction patterns from ultrathin iron films on Ag(001) for some selected overlayer thicknesses.